Influence of fuel ash on the recoverability of copper from the spent material of chemical looping combustion

*Jinze Dai, Logan Hughey, Kevin J. Whitty**

Department of Chemical Engineering, The University of Utah, 50 South Central Campus Drive, MEB Room 3290, Salt Lake City, Utah 84112, United States

* Corresponding author. E-mail address: kevin.whitty@utah.edu.

Abstract: Chemical looping combustion (CLC) is an advanced energy production technology that inherently separates the CO_2 generated. The oxygen needed for fuel conversion is supplied by the oxygen carrier. When using copper-based oxygen carriers, oxygen carrier attrition is a challenge to the process economics, unless the attrited copper that is mixed with fuel ash in the spent material can be recovered by, for instance, acid leaching. However, fuel ash may transform the attrited copper into certain complexes of low leachability (e.g., $CuAl_2O_4$), hindering the copper recovery. In this study, the copper content in the spent material was first evaluated. The effects of ash composition and copper content on the occurrence mode of copper in spent material were predicted by thermodynamic modeling. Redox cycles of simulated spent materials based on various coal ashes were performed to reveal the characteristics of $CuAl_2O_4$/$CuFe_2O_4$

formation. The CuO-Al_2O_3 reaction was investigated under the temperatures and solid residence times experienced in CLC. The materials were analyzed by X-ray diffraction. The results suggest that the fuel ash with a high Al/Ca ratio may lower the recoverability of copper when the temperature is above 925°C. The slow formation of $CuFe_2O_4$ is not expected to affect the copper recovery.

Keywords: Chemical looping; Ash; Recovery; Spent material; Thermodynamic modeling; Attrition.

1. Introduction

To lower the cost and energy penalty of carbon capture, chemical looping combustion (CLC) has been extensively studied [1–5]. CLC employs oxygen carriers to transfer the oxygen from the air to the fuel to avoid direct air/fuel contact. As a result, the CO_2 generated from fuel combustion would be inherently separated from the N_2 derived from air. As shown in **Fig. 1**, a CLC system builds on two interconnected reactors, including the air reactor (AR) and the fuel reactor (FR). The oxygen carrier (metal oxide, Me_xO_y) circulates between the two reactors (typically fluidized-beds), receiving the oxygen from air in AR and delivering the oxygen to combust the fuel in FR. For the conversion of solid fuels, there are generally three types of oxygen carriers with different modes of oxygen supply. The oxygen carriers used in the iG-CLC process only provide lattice oxygen to oxidize the syngas derived from the in-situ gasification of solid fuels. Iron-based and calcium-based oxygen carriers fall under this category. On the other hand, the oxygen carriers for chemical looping with oxygen uncoupling (CLOU) are based on the metal oxides that can self-decompose and release gaseous oxygen at desired temperatures, e.g., CuO and Mn_2O_3. Besides, the oxygen carriers composed of both iG-CLC and CLOU

oxygen-carrying materials serve for chemical looping assisted by oxygen uncoupling (CLaOU), such as Fe-Mn bimetallic oxides. As pointed out by Adánez and Abad [6], to eliminate the oxygen demand required to burn off the volatiles/syngas escaping from FR, the use of pure CLOU oxygen carrier is a solution. Also, Stevens et al. [7] reported that the estimated net plant efficiency of CuO-based CLOU system (35.6%, HHV) is higher than that of Fe_2O_3-based CLC system (33.3%, HHV). Considering the capability of CuO to achieve high fuel conversion and high carbon capture efficiency with low solid inventory [8–12], this study is dedicated to copper-based oxygen carriers.

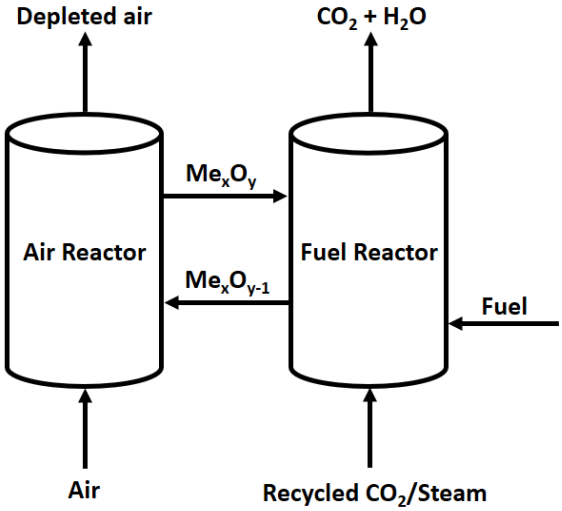

Fig. 1. Principle of CLC process for carbon capture.

From the perspective of process economics, it is desirable to recover and recycle the copper leaving the reactors to minimize the cost of oxygen carrier makeup. Although ideally the inventory of oxygen carrier in the reactors should be constant to ensure high carbon capture efficiency, the loss of oxygen-carrying material through attrition/fragmentation and particle elutriation from the reactor outlets is inevitable. Therefore, oxygen carrier makeup is necessary. However, using fresh oxygen carrier to make up for the lost material may not be economically viable, especially for high-cost oxygen carriers such as copper-based ones for solid fuel

combustion. Even for the natural ore oxygen carriers that are much cheaper than copper-based oxygen carriers, the cost of oxygen carrier makeup without recovery and recycling could be substantial. For instance, according to Lyngfelt and Leckner [13], the makeup costs related to ilmenite (175 €/ton, lifetime=200 h) and manganese ore (225 €/ton, lifetime=100 h) were estimated to be around 2 €/ton CO_2 and 5 €/ton CO_2 avoided, respectively. In a more optimistic estimation, assuming 50% of the spent oxygen carrier is recovered and recycled, the oxygen carrier that costs 1500 €/ton with a lifetime of 1250 h would add 3.3 €/ton CO_2 avoided [14]. When it comes to copper-based oxygen carriers, the fresh material is supposed to cost at least \$6600/ton CuO in 2019 (raw copper ore) [15], a considerable increase over the price of \$2900/ton CuO in 2006 when Abad et al. [16] performed the economic analysis. For commercially manufactured synthetic oxygen carriers, the price could be 1-2 orders of magnitude higher [17]. A more detailed analysis on the cost for the makeup of copper-based oxygen carrier using fresh material while burning Powder River Basin (PRB) sub-bituminous coal is presented in **Fig. 2**. The minimum cost of oxygen carrier (OC) makeup in this case can be expressed by

$$CCC_{OC,min} = \frac{C_{OC,min} SSI}{SE \eta_{CO2} LT} \quad (1)$$

where $CCC_{OC,\,min}$ is the minimum cost of OC makeup per ton of CO_2 captured (\$/ton CO_2 captured), $C_{OC,\,min}$ is the minimum unit cost of fresh OC on the CuO-equivalent basis (\$6600/ton CuO), SSI refers to the specific solid inventory (0.4 ton CuO/MW_{th} [18]), SE is the specific emission of PRB coal (0.326 ton CO_2/MWh_{th}), η_{CO2} is the assumed CO_2 capture efficiency (98%), LT represents the average lifetime of the oxygen carrier, which is the key variable. It can be seen that to limit the cost of OC makeup with fresh material to below \$10/ton CO_2, the lifetime of OC must be longer than 800 h, i.e., the OC attrition rate has to be lower than

0.125%/h. However, according to the published works, it is difficult to guarantee the OC attrition rate is below 0.125%/h when combusting solid fuels at >900°C under chemical, mechanical, and thermal stresses. In Technische Universität Darmstadt's 1 MW_{th} CLC pilot plant, the attrition rates of ilmenite and iron ore were found to be 0.4-2.3%/h [19]. The 50 kW_{th} CLC system at U.S. National Energy Technology Laboratory using CuO-Fe_2O_3 bimetallic oxygen carrier experienced an overall attrition rate of about 1%/h under autothermal conditions [20]. The attrition rate of hematite under high temperature and reacting conditions was measured to be 0.2-1.2%/h [21]. Nelson at el. [22] found that as the temperature increased from 895°C to 970°C, the attrition rate of ilmenite increased from 0.9%/h to 3.2%/h. For a bauxite cement-bonded Fe-based oxygen carrier, the mean attrition rate was 0.26%/h [23]. The attrition rate of MgO-kaolin-supported manganese ores were 2.2 %/h [24]. Of the five copper-based synthetic oxygen carriers tested in a 500 W_{th} unit firing CH_4 at 900°C, only two displayed attrition rates below 0.125%/h [25]. In summary, the option of OC makeup using the copper recovered from spent material deserves further attention.

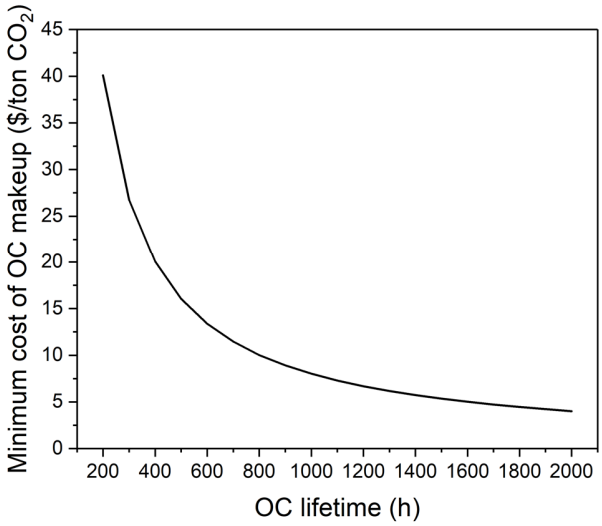

Fig. 2. Minimum cost of OC makeup using fresh material for copper-based CLC.

The main challenge of copper recycling for CLC lies in the separation of the attrited copper from the fuel ash. Although the copper exiting AR can be easily collected by the filtration device and then be reused, it was reported that the attrition rate of OC in FR was much higher than that in AR when burning natural gas, and 92.4 wt.% of the solids elutriated from FR were fines instead of large particles [20]. For the CLC firing solid fuels, the FR attrition rate is expected to be even higher due to the collisions between OC particles and fuel/ash particles along with higher solid inventory in FR. Therefore, the recovery and recycling should primarily target the copper escaping the FR cyclone, which is accompanied by the flue gas and fly ash. The downstream filtration device will collect this kind of copper together with the ash, forming the spent material to be discharged. One possible way to recover the copper mixed with ash is by acid leaching: copper oxides are supposed to be much more leachable than the ash components such as quartz, corundum, and aluminosilicates. In fact, acid leaching is a common method for the recovery of copper from the spent materials of other industries [26,27]. However, if the interaction between ash and attrited fines turns the copper into $CuAl_2O_4$/$CuAlO_2$, the recovery of

copper will be hindered, as $CuAl_2O_4$/$CuAlO_2$ are much less leachable than CuO/Cu_2O [28]. As demonstrated in **Fig. 3**, there are three mechanisms by which the ash may influence the attrited copper. Mechanism 1: The ash particles capture the attrited fines, triggering the interaction. Mechanism 2: the attrited fines are received by the burning char, which will burn out and expose the ash/copper oxide mixture. Mechanism 3: the ash particles deposit on the surface of the oxygen carrier, which then undergoes attrition. Previous studies regarding the ash/CuO interaction mainly concerned the long-term impact of bottom ash on the redox reactivity and oxygen transport capacity of the CuO staying in the reactors, featuring high Cu concentrations in the ash/CuO mixtures and long interaction time [29–33]. It was found that the coal ashes with high Al/Ca and Fe/Ca ratios can form $CuAl_2O_4$ and $CuFe_2O_4$ with CuO [34,35]. Nevertheless, the content and occurrence mode of copper in the spent material, which are crucial to the recoverability of copper, remains unclear.

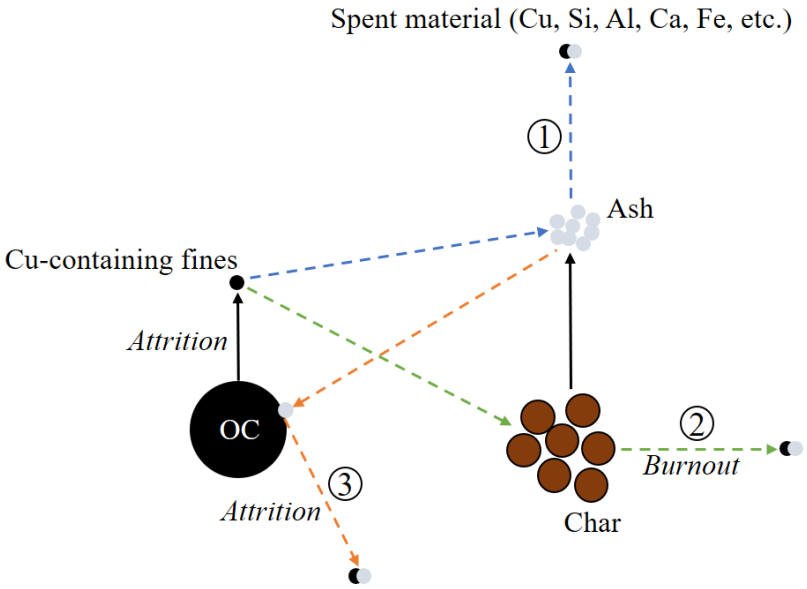

Fig. 3. Potential mechanisms by which the fuel ash influences the attrited copper.

The objective of this work is to demonstrate the influence of fuel ash on the recoverability of copper from the spent material. Based on mass balance calculation, thermodynamic modeling,

high-temperature experiments, and XRD analysis, the risk of fuel ash transforming the copper into the non-leachable form is systematically assessed in this work, which will facilitate the development of the copper recovery and recycling process, improving the economic competitiveness of copper-based CLC technology.

2. Materials and methods

2.1. Materials

The simulated spent material was prepared by mixing CuO powder (Alfa Aesar, <74 μm) with fuel ash (<106 μm). To obtain representative fuel ashes, two types of pulverized coal were combusted, including Powder River Basin (PRB) sub-bituminous coal and Illinois #6 (IL6) bituminous coal. The proximate/ultimate analyses and ash compositions of PRB and IL6 are given in Table 1. The coal combustion was performed at 900°C in a muffle furnace under air for 4 hours. The coal ash from air combustion should be equivalent to the coal ash from CLOU's FR, as the overall gas atmospheres of CLOU's FR and air combustion are both oxidizing so that the ash compounds are in oxidized state.

Table 1. Proximate/ultimate analyses and ash compositions of the fuels.

Coal Analysis (as received basis, wt.%)			Ash Analysis (wt.%)		
	PRB	IL6		PRB	IL6
C	56.17	64.67	Al_2O_3	15.20	17.66
H	3.78	4.52	CaO	18.55	1.87
N	0.80	1.12	Fe_2O_3	5.73	14.57
S	0.25	3.98	MgO	4.47	0.98
O	15.81	8.07	P_2O_5	1.08	0.11
Moisture	18.24	9.65	K_2O	0.48	2.26
Ash	4.95	7.99	SiO_2	33.63	49.28
Volatiles	37.88	36.78	Na_2O	1.59	1.51
Fixed Carbon	38.93	45.58	SO_3	9.27	2.22
HHV (MJ/kg)	22.26	26.98	TiO_2	1.30	0.85

In addition, Al_2O_3 powder (SASOL Germany GmbH) was used in this study to assess the formation rate of $CuAl_2O_4$ spinel at CLOU temperatures (900-950°C).

2.2. Estimation of copper content in the spent material based on mass balance

To evaluate the recoverability of copper from spent material, it is essential to first figure out the probable range of copper content in spent material. The preliminary estimation is focused on the FR side where the spent material is generated. The copper is assumed to be in the cupric form (Cu^{2+}) in the spent material, no matter whether it bonds with ash compounds or not. There are two main reasons for this assumption. First, to achieve complete solid fuel combustion, an oxygen carrier-to-fuel ratio (ϕ) of greater than 3 is recommended in recent literature [36,37]. Theoretically, less than 33.3% of the CuO will be reduced into Cu_2O while over 66.7% still remains as CuO in FR. Second, different from the bulk Cu_2O being conveyed down to the AR after oxygen release, the attrited Cu_2O will flow upward and likely be re-oxidized by the excess O_2 in the upper region of FR. Two major components in spent material were considered in the calculations, including the copper oxide resulting from attrition and the fuel ash. In theory, the concentrations of unburnt char and inert support material are negligible in the spent material. Even if char and support material are present, they should not affect the occurrence mode of copper. Ideally, the fuel ash is supposed to leave the FR together with the flue gas and then be captured by the filter, thereby no ash is accumulating inside the FR, i.e., 100% of the ash ends up as fly ash. Hence, for preliminary estimation, the content of copper in the spent material ($y_{Cu,spent}$, wt.%) can be expressed as follows:

$$y_{Cu,spent} = \frac{SI_{Cu,FR} r_{attr,FR}}{SI_{Cu,FR} r_{attr,FR} M_{CuO}/M_{Cu} + \dot{m}_{fuel} y_{ash}} \times 100\% \quad (2)$$

where $SI_{Cu,FR}$ is the solid inventory of Cu in the FR (kg), $r_{attr,FR}$ refers to the attrition rate of OC in FR (%/h), $\dot{m}_{fuel}$ represents the fuel feeding rate (kg/h), and y_{ash} is the ash content in fuel

(wt.%). M_{CuO} and M_{Cu} are the molar masses of CuO (79.55 kg/kmol) and Cu (63.55 kg/kmol), respectively. Furthermore, $SI_{Cu,FR}$ can be written as

$$SI_{Cu,FR} = \frac{\dot{m}_{fuel}\Omega_{fuel}\phi\tau_{FR}M_{Cu}}{R_{CuO}M_{CuO}} \quad (3)$$

where Ω_{fuel} is the stoichiometric amount of O_2 required to burn the fuel (kg O_2/kg fuel), R_{CuO} refers to the oxygen transport capacity of CuO (0.10 kg O_2/kg CuO), ϕ is the oxygen carrier-to-fuel ratio, and τ_{FR} is the mean residence time of OC in FR (h). Consequently, Equation (2) can be reduced into

$$y_{Cu,spent} = \frac{8\Omega_{coal}\phi\tau_{FR}r_{attr,FR}}{10\Omega_{coal}\phi\tau_{FR}r_{attr,FR}+y_{ash}} \times 100\% \quad (4)$$

The value of Ω_{fuel} is typically in the range of 1.2-2.0 depending on the fuel composition [38]. For PRB coal, Ω_{fuel} is 1.64 kg O_2/kg coal, which is a medium value and used in this study. In addition, the ϕ and τ_{FR} are set to be 3 and 0.0333 h (2 min) [18], respectively. The ranges of the key variables are selected to be 0.1-1.0%/h for $r_{attr,FR}$ and 5-15% for y_{ash}.

2.3. Thermodynamic Modeling

To predict the occurrence mode of copper in the spent material, thermodynamic modeling was conducted using FactSage 7.3 software. The equilibrium composition of the spent material with minimized Gibbs energy was calculated. In addition to the built-in databases FactPS and FToxid, a user-defined database including Cu-containing complexes such as $CuAl_2O_4$, $CuAlO_2$, Ca_2CuO_3, and $CaCuO_2$ was employed. The thermodynamic data needed to define these Cu-containing complexes in the database was from the literature [39,40].

There were two variables in the thermodynamic calculations. The first was the composition of ash. The ash compositions of PRB and IL6 from Table 1 were used for comparison. The copper content in the spent material was the other variable, which was varied within the estimated range

according to Section 2.2. The gas atmosphere was set to be oxidizing at 1 atm, and the temperature was 900°C. It should be pointed out that the thermodynamic modeling can only present the equilibrium composition of the spent material without considering the kinetics, while the interaction time of fuel ash and attrited copper in the high-temperature region of FR is limited, presumably not longer than the solid residence time in FR. However, the thermodynamic modeling is still useful in predicting the maximum amount of copper transformed into $CuAl_2O_4$ and $CuFe_2O_4$, reflecting the worst-case scenario. In addition, the predicted oxygen transport capacity of the spent material can be compared with the experimental results in Section 2.4.

2.4. Redox cycles of simulated spent materials: revealing the formation of $CuAl_2O_4$ and $CuFe_2O_4$

The redox cycles of simulated spent materials performed in thermogravimetric analyzer (TGA) can reveal the formation of $CuAl_2O_4$ or $CuFe_2O_4$. Specifically, our previous studies demonstrated that the formation of $CuAl_2O_4$ in coal ash/CuO mixture resulted in a decreasing oxygen transport capacity of the mixture as $CuAl_2O_4$ cannot release gaseous oxygen at normal CLOU temperatures; the decomposition of the $CuFe_2O_4$ formed would display an additional weight loss peak in the DTG curve, which can be differentiated from the primary weight loss peak of CuO decomposition [34,35]. In this work, the oxygen transport capacity of the simulated spent material was defined as the weight gain during the oxidation stage of a redox cycle divided by the initial weight of the material. The DTG curve (dm/dt) is the first derivative of the mass-time curve.

The redox cycles were performed in the Q600 TGA manufactured by TA instruments, which was equipped with a reference pan to offset the buoyancy effect, attaining superior accuracy. 20 mg simulated spent material composed of coal ash (PRB/IL6) and CuO with a specific copper content (8%/12%/16%) was loaded in the sample pan. The simulated spent material was first

heated to the target temperature (900°C or 925°C) at 30°C/min under CO_2 gas flow (300 mL/min) to trigger the decomposition of CuO ($4CuO \rightarrow 2Cu_2O + O_2$), then the inlet gas was switched from CO_2 to air (300 mL/min) to allow for the oxidation of Cu_2O ($2Cu_2O + O_2 \rightarrow 4CuO$), which constitutes a redox cycle. To ensure the reactions are complete, every redox cycle had 60 min of reduction and 20 min of oxidation at the target temperature. 5 redox cycles were carried out for each test. To show the data reproducibility, each test was repeated three times.

2.5. Assessing the risk of $CuAl_2O_4$ formation in realistic time frame under iso-thermal condition

The formation of $CuAl_2O_4$ from the reaction between CuO and ash-derived Al_2O_3 is the most concerning influence that fuel ash could have on the recoverability of copper. To assess the intrinsic formation rate of $CuAl_2O_4$, it is necessary to control the reaction time under iso-thermal condition. The CuO/Al_2O_3 mixture (20 mg) with a molar ratio of 1:1 was loaded in a ceramic boat and sent into an electric furnace (Thermolyne, Thermo Scientific) that had already been heated to high temperature (900-950°C). After a controlled period of time (2-5 min), the mixture was withdrawn from the furnace and subject to visual inspection and XRD analysis.

2.6. XRD analysis of simulated spent materials and CuO/Al_2O_3 mixtures after heat treatment

To directly confirm the formation of $CuAl_2O_4/CuFe_2O_4$ in simulated spent materials and CuO/Al_2O_3 mixtures during thermal treatment, XRD analysis was conducted using Bruker D2 PHASER. The CuKα radiation was operated at 30 kV and 10 mA. The 2θ was in the range of 10-70° with a step size of 0.02°. The crystalline phases were identified using DIFFRAC.EVA software with Crystallography Open Database (COD) and Powder Diffraction File (PDF) for reference patterns.

3. Results and discussion

3.1. Estimated range of copper content in the spent material

Fig. 4 shows the estimated copper contents in the spent material under various attrition rates for different ash contents. As expected, the copper content increases with increasing attrition rate and decreasing ash content, exhibiting a high sensitivity to both factors. On one hand, if the FR attrition rate is as high as 1.0%/h, the spent material could contain up to 20 wt.% of copper. On the other hand, under relatively low attrition rates (<0.2%/h), the copper content in spent material is expected to be lower than 5 wt.%, even for an ash content of 5 wt.%. In summary, when the attrition rate is concerning (>0.2%/h), the percentage of copper in the spent material should be high enough to warrant recovery efforts.

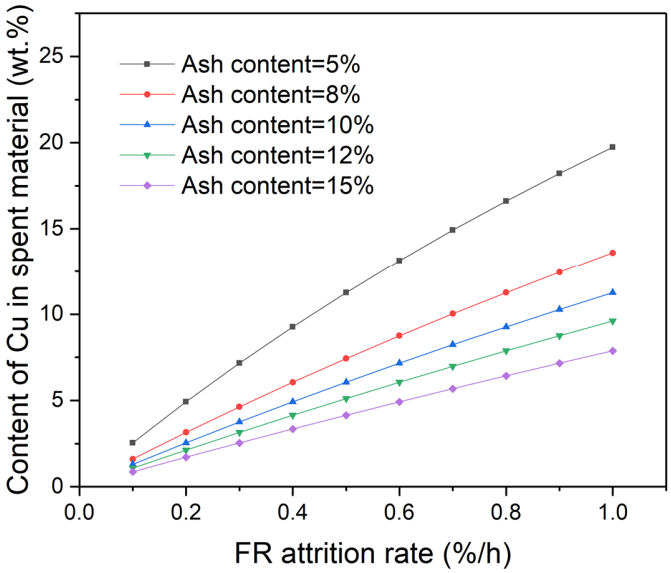

Fig. 4. Estimated content of copper in the spent material.

3.2. Characteristics of $CuAl_2O_4$/$CuFe_2O_4$ formation in the simulated spent materials: effects of ash composition, copper content, and temperature

Fig. 5 illustrates the equilibrium distribution of copper between CuO, $CuAl_2O_4$, and $CuFe_2O_4$ for the spent materials based on PRB ash or IL6 ash with varying copper contents. The spent

material based on PRB ash would not contain $CuAl_2O_4$ or $CuFe_2O_4$, while IL6 ash can lead to the formation of $CuAl_2O_4$ and $CuFe_2O_4$. In the case of IL6 ash, when the copper content is lower than 8 wt.%, the ash would be over-stoichiometric, i.e., if the attrition rate is below 0.55%/h, the Al and Fe in ash have the potential to turn all of the attrited Cu into Cu-Al and Cu-Fe complexes. On the other hand, once the copper content reaches 10 wt.%, the CuO will be in excess, hence the amount of $CuAl_2O_4$ and $CuFe_2O_4$ that can be formed theoretically only depends on the availability of Al and Fe. Specifically, the predicted ratio of the Cu as $CuFe_2O_4$ to the Cu as $CuAl_2O_4$ is constant (=1.35) with excess CuO. In summary, the theoretical amount of $CuAl_2O_4$ and $CuFe_2O_4$ in equilibrium is governed by both the ash composition and the copper content in spent material. Since the proportion of copper that can potentially be transformed into $CuAl_2O_4$ and $CuFe_2O_4$ is significant in equilibrium, it is important to investigate the kinetics of $CuAl_2O_4$/$CuFe_2O_4$ formation to assess the extent of reaction in reality.

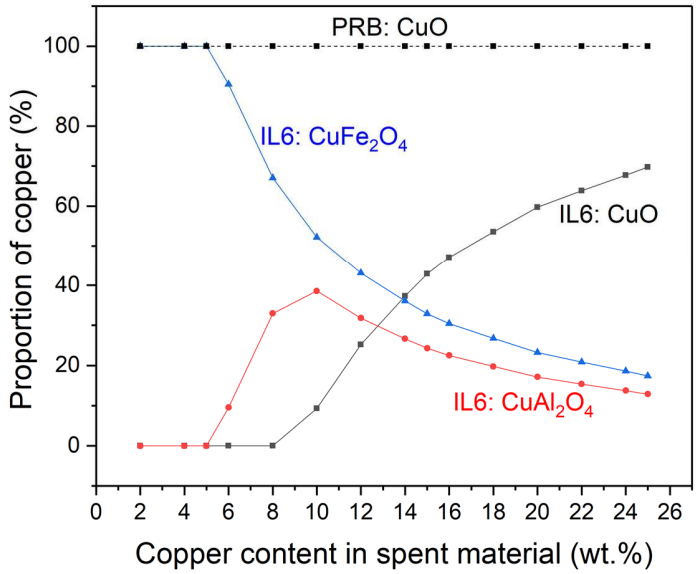

Fig. 5. Equilibrium distribution of copper in spent materials as a function of copper content.

To test the modeling predictions in **Fig. 5**, the oxygen transport capacities of the simulated spent materials were measured by TGA redox cycles. The PRB ash-based spent material is compared with the IL6 ash-based spent material in **Fig. 6**. The copper contents of the simulated spent materials presented in **Fig. 6** were 16 wt.% (20 wt.% CuO), corresponding to a theoretical oxygen transport capacity of 2 wt.% when no $CuAl_2O_4$ is formed. Apparently, the oxygen transport capacity of the PRB ash-based spent material was constantly very close to 2 wt.% (the predicted value), confirming that $CuAl_2O_4$ did not form. On the other hand, the oxygen transport capacity of the IL6 ash-based spent material was considerably lower than 2 wt.% after the first cycle. The transport capacity then decreased with each redox cycle, approaching the value predicted by thermodynamic modeling, which suggests that $CuAl_2O_4$ was generated as expected. It is now clear that the formation of $CuAl_2O_4$ in the spent material depends on the ash composition. To quickly predict whether a certain ash could cause the formation of $CuAl_2O_4$, the threshold proposed in our previous work can be used: any ash with a Al_2O_3/CaO mass ratio

higher than 1.82 is higher risk, because the amount of Ca is too little to combine with and consume the Al, enabling the excess Al to react with CuO [34]. In this study, the Al_2O_3/CaO ratio of IL6 ash (9.44) is much higher than that of PRB ash (0.82).

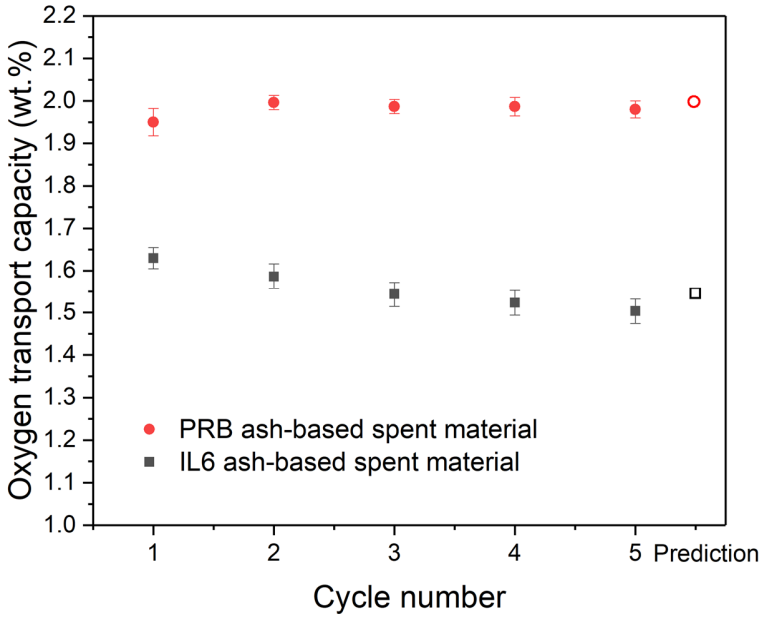

Fig. 6. Oxygen transport capacities of simulated spent materials over redox cycles.

As shown in **Fig. 7(a)**, for the IL6 ash-based simulated spent materials containing 8 wt.%, 12 wt.%, and 16 wt.% of copper, the oxygen transport capacities at the fifth redox cycle were all close to the predicted values. It should be noted that in the first cycle, the oxygen transport capacity of the 16 wt.% copper material had already dropped by 19%, which was not far from the predicted decrease of 23% in equilibrium. Similarly, the simulated spent materials containing 8% and 12% of copper also experienced a significant loss of oxygen transport capacity in the first cycle (decrease by 20% and 19%, respectively). The results above imply that the formation of $CuAl_2O_4$ in the spent material is significant in the first cycle and not sensitive to the copper content, and the amounts of $CuAl_2O_4$ formed at the end were consistent with the modeling

predictions, i.e., the $CuAl_2O_4$ formation is not slow. On the contrary, according to the DTG curves in **Fig. 7(b)**, the formation of $CuFe_2O_4$ seems to be slow and differ from modeling predictions. The downward peaks in the DTG curves indicate weight loss, while the upward peaks mean weight gain. The spikes were due to the switch of inlet gas. With a copper content of 16 wt.%, there was no obvious secondary weight loss peak of $CuFe_2O_4$ decomposition until the third redox cycle, after which the secondary peak grew slowly. With a lower copper content (8 wt.%), the secondary peak was hardly visible even at the fifth redox cycle, which contradicts the modeling prediction that 67% of the copper was supposed to be in the form of $CuFe_2O_4$. It appears that the reaction between ash-derived Fe_2O_3 and CuO was limited not only by the slow kinetics but also by the solid-solid contact when the copper content was low. This is probably because the Fe_2O_3 in IL6 ash originated from pyrite (FeS_2) was present as large discrete particles with small specific surface area, hence it was hard for the CuO to access Fe_2O_3 under low copper content.

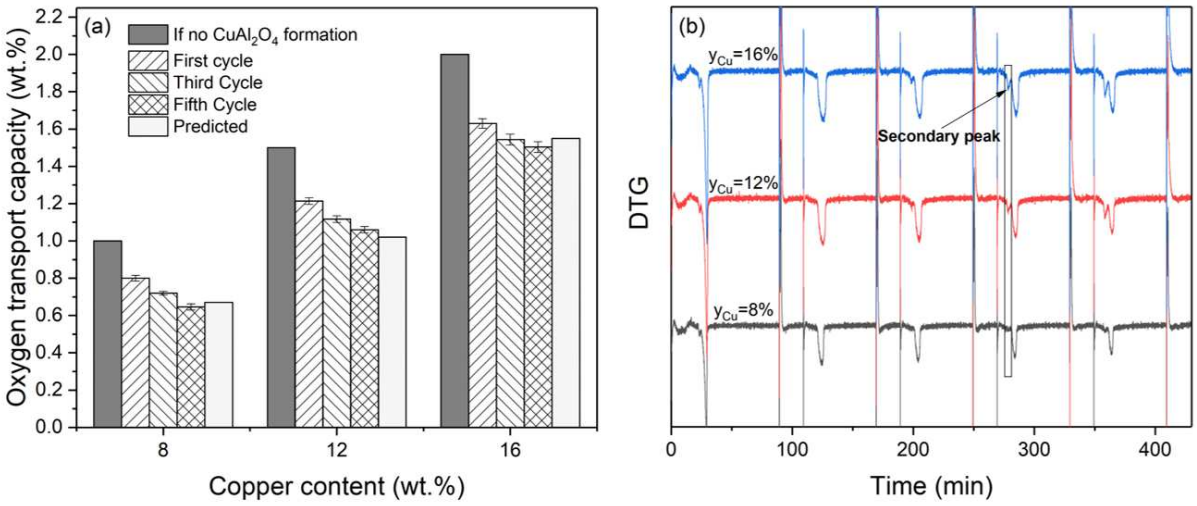

Fig. 7. Predicted and measured oxygen transport capacities (a) and DTG curves (b) of IL6 ash-based spent materials with various copper contents at 900°C.

Although increasing the temperature to 925°C promoted the formation of $CuFe_2O_4$, the Fe_2O_3-CuO reaction in the spent material was still not intense in the first 120 minutes even with 16 wt.% copper. As shown in **Fig. 8**, at 925°C, the secondary weight loss peaks after the third redox cycle were much stronger than at 900°C. However, the secondary peak still did not arise in the first two redox cycles even at 925°C. Given the probable residence time of spent material at CLOU temperature being within several minutes (no longer than the mean residence time of OC in FR), the spent material is not likely to contain $CuFe_2O_4$, while the formation of $CuAl_2O_4$ is possible.

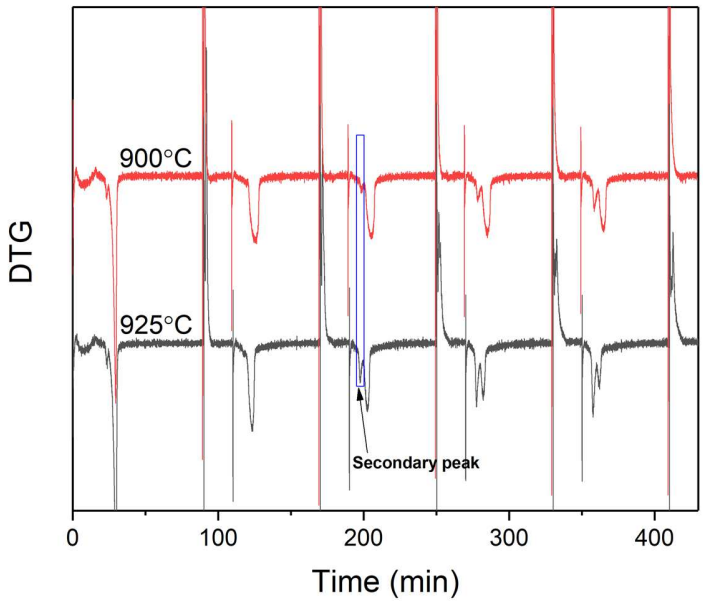

Fig. 8. DTG curves of IL6 ash-based spent material with 16 wt.% Cu at different temperatures.

XRD analysis supports the observations from the redox cycle analysis. The IL6 ash-based simulated spent materials were scanned by XRD following the first and fifth redox cycle. For a straightforward presentation, only the characteristic peak of a certain species (the strongest peak without overlapping with the peaks of any other species) was labeled in the XRD patterns in **Fig. 9**. According to **Fig. 9**(a), at 900°C, after the first redox cycle, the peak of Fe_2O_3 was strong and the peak of $CuFe_2O_4$ was nearly absent, proving that the Fe_2O_3 in ash was not efficiently transformed into $CuFe_2O_4$ in the first cycle. Meanwhile, a significant peak of $CuAl_2O_4$ was detected after the first cycle, confirming $CuAl_2O_4$ was already formed in the first cycle. The discrepancy between the $CuFe_2O_4$ formation and $CuAl_2O_4$ formation in the first cycle revealed by XRD analysis explains the observations from the corresponding TGA measurement: significant CuO deactivation occurred in the first cycle because of the $CuAl_2O_4$ formation, while the secondary weight loss peak is invisible until the third cycle due to the absence of $CuFe_2O_4$.

Therefore, the formation of $CuFe_2O_4$ in the spent material is found to be much slower than that of $CuAl_2O_4$. When it came to the fifth cycle, the peak of $CuFe_2O_4$ arose, while the peak of Fe_2O_3 was largely suppressed, suggesting the conversion from Fe_2O_3 to $CuFe_2O_4$. Also, the characteristic peak of $CuAl_2O_4$ after 5 cycles was stronger than that after 1 cycle: more $CuAl_2O_4$ was formed, resulting in decreasing oxygen transport capacity. For the material containing 8 wt.% Cu, even after 5 redox cycles, the Fe_2O_3 peak remained very strong, and the $CuFe_2O_4$ peak was very weak. Nonetheless, the $CuAl_2O_4$ peak displayed high intensity, similar to the case of 16 wt.% Cu/5 cycles. Hence, it was confirmed that a low copper content would hinder the formation of $CuFe_2O_4$ but not inhibit the formation of $CuAl_2O_4$. As shown in **Fig. 9**(b) , the XRD patterns of the simulated spent materials at 925℃ were noisy, probably due to the partial melting that lowered the crystallinity of the components. However, the trends at 900°C can also be seen at 925°C: relatively strong Fe_2O_3 peak and weak $CuFe_2O_4$ peak after the first cycle, and the notable $CuFe_2O_4$ peak after the fifth cycle. At 900°C, though very weak, the Fe_2O_3 peak still existed after 5 redox cycles, while at 925℃, it disappeared after 5 redox cycles, indicating that the CuO-Fe_2O_3 reaction was more intense at 925°C.

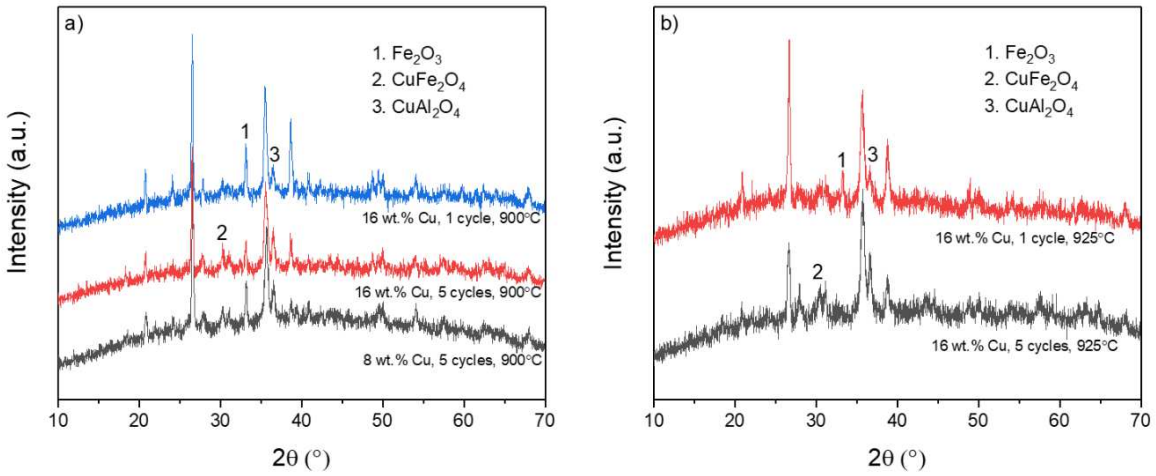

Fig. 9. XRD patterns of IL6 ash-based simulated spent materials.

3.3. Formation of $CuAl_2O_4$ in the realistic time frame (2-5 min)

Considering the results above, the formation of $CuFe_2O_4$ in the spent material is not expected to be severe under FR conditions in several minutes of residence time. The focus then shifts to determining whether or not $CuAl_2O_4$ formation is significant in the realistic time frame. To check whether the formation of $CuAl_2O_4$ would be appreciable under isothermal conditions in 2-5 min, the CuO/Al_2O_3 mixtures were directly sent to a furnace already heated to 900-950°C for 2-5 min without the temperature ramping step. The initial mixture of CuO (black color) and Al_2O_3 (white color) is grey in color, while the color of $CuAl_2O_4$ is chocolate brown [41]. Therefore, the formation of $CuAl_2O_4$ can be easily recognized by visual inspection: the color change of the material from grey to brown implies that $CuAl_2O_4$ was generated during the isothermal heat treatment. As demonstrated in **Fig. 10**, the color change was more pronounced as the temperature and residence time increased. In particular, it took 5, 3, and 2 min for the material to display a significant color change when the temperature was 900, 925, and 950°C, respectively. The XRD results (**Fig. 11**) were consistent with the findings of visual inspection:

the intensity of the $CuAl_2O_4$ peak was positively correlated with the temperature and residence time. At 900°C, the $CuAl_2O_4$ peak was very weak for both 2 min and 3 min. At 925°C, there was a notable $CuAl_2O_4$ peak at 3 min. When the temperature was raised to 950°C, the $CuAl_2O_4$ peak emerged after merely 2 min and became substantial after 3 min. Since the residence time of spent material in the FR is not likely to exceed 5 min, the formation of $CuAl_2O_4$ should be minimal at 900°C. However, if the temperature reaches 950°C, a substantial amount of CuO will be transformed into $CuAl_2O_4$ in 3 min. Therefore, 925°C should be thought of as a temperature threshold: above 925°C, the increase in $CuAl_2O_4$ content may reduce the recoverability of copper.

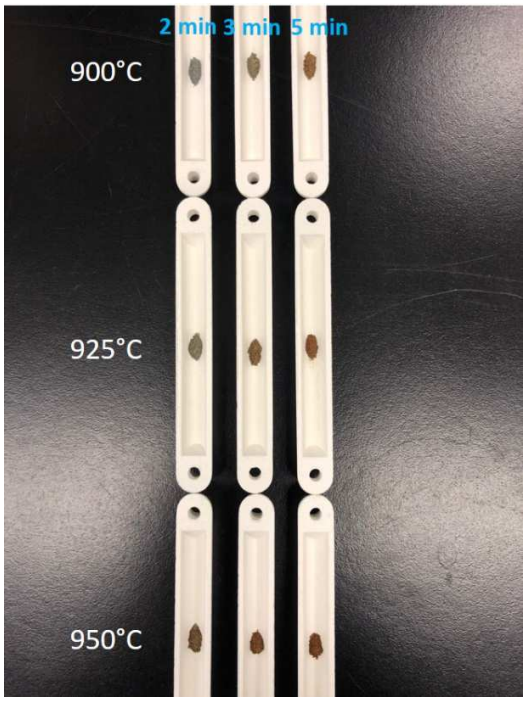

Fig. 10. Photos of CuO/Al_2O_3 mixture after heat treatment at various temperatures for different residence times.

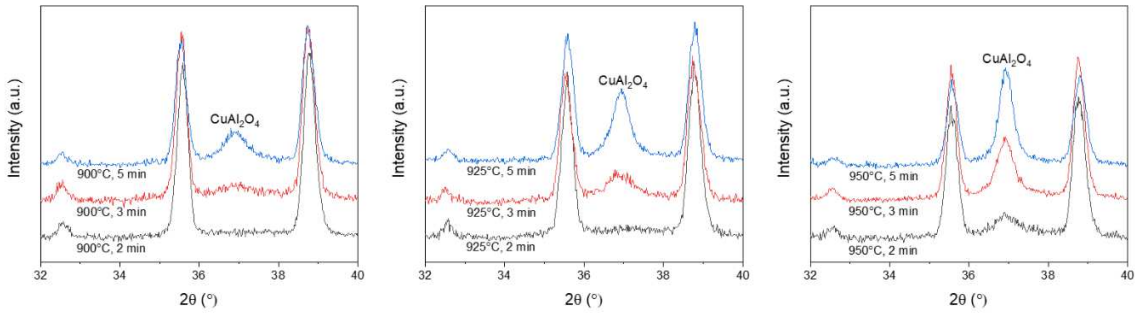

Fig. 11. XRD patterns of CuO/Al_2O_3 mixture after heat treatment at various temperatures for different residence times.

From a practical perspective, the properties of the fuel used (reactivity/ash composition/ash content) should match the attrition resistance of the OC. When the OC happens to be of high attrition rate so that the amount of copper to be recovered is very large, the fuel used should ideally meet at least one of the two standards below: (1) the fuel is reactive enough to be efficiently converted at <925°C; (2) the ash is of low Al_2O_3/CaO mass ratio, preferably lower than 1.82. If the conversion of the fuel requires >925°C and its ash contains excess Al, adding CaO or co-firing with a high-Ca fuel to inhibit the formation of $CuAl_2O_4$ could be an option, according to the general principle proposed in our previous work [34].

4. Conclusions

Based on mass balance calculations, thermodynamic modeling, TGA redox cycles, isothermal solid-solid reaction experiments, and XRD analysis, the influence of fuel ash on the recoverability of copper from the spent material of CuO-based chemical looping combustion was systematically investigated. The findings are essential in the continuous effort to reduce the cost of carbon capture in chemical looping systems. The conclusions are summarized as follows:

(1) The content of copper in the spent material is estimated to be in the range of 2-20 wt.% under probable FR attrition rates (0.2-1%/h) and ash contents (5-15 wt.%).

(2) The occurrence mode of copper in the spent material depends on the ash composition, copper content, and temperature. The simulated spent material based on PRB ash does not contain $CuAl_2O_4$ and $CuFe_2O_4$ after extended heat treatment, while the counterpart based on IL6 ash contains $CuAl_2O4$ and $CuFe_2O_4$. The formation of $CuAl_2O_4$ and the oxygen transport capacity of the simulated spent material based on IL6 ash can be accurately predicted by thermodynamic modeling. Although high temperature and high copper content facilitate the CuO-Fe_2O_3 reaction, the formation of $CuFe_2O_4$ in the spent material is much slower than that of $CuAl_2O_4$. Given that the realistic residence time of spent material in the FR is on the order of minutes, $CuFe_2O_4$ should not be prevalent in the spent material.

(3) The CuO-Al_2O_3 reaction is sensitive to temperature. When burning a fuel with a high Al/Ca ratio at >925°C, the fuel ash may turn the attrited copper into $CuAl_2O_4$, lowering the recoverability of the copper in spent material.

Acknowledgement

This material is based upon work supported by the Department of Energy under Award Number DE-FE0029160. The views and opinions of authors expressed herein do not necessarily state or reflect those of the United States Government or any agency thereof. Dr. Dan Gall is gratefully acknowledged for the suggestions on this work. Dana Overacker is appreciated for the assistance in the experiments.

References

[1] T. Mattisson, M. Keller, C. Linderholm, P. Moldenhauer, M. Rydén, H. Leion, A. Lyngfelt, Chemical-looping technologies using circulating fluidized bed systems : Status

of development, Fuel Process. Technol. 172 (2018) 1–12. doi:10.1016/j.fuproc.2017.11.016.

[2] J. Adánez, A. Abad, T. Mendiara, P. Gayán, L.F. de Diego, F. García-Labiano, Chemical looping combustion of solid fuels, Prog. Energy Combust. Sci. 65 (2018) 6–66. doi:10.1016/j.pecs.2017.07.005.

[3] I. Adánez-rubio, A. Pérez-astray, T. Mendiara, M. Teresa, A. Abad, P. Gayán, L.F. De Diego, F. García-labiano, J. Adánez, Chemical looping combustion of biomass : CLOU experiments with a Cu-Mn mixed oxide, Fuel Process. Technol. 172 (2018) 179–186. doi:10.1016/j.fuproc.2017.12.010.

[4] A. Lyngfelt, Chemical-looping combustion of solid fuels - Status of development, Appl. Energy. 113 (2014) 1869–1873. doi:10.1016/j.apenergy.2013.05.043.

[5] L.S. Fan, F. Li, Chemical looping technology and its fossil energy conversion applications, Ind. Eng. Chem. Res. 49 (2010) 10200–10211. doi:10.1021/ie1005542.

[6] J. Adánez, A. Abad, Chemical-looping combustion : Status and research needs, Proc. Combust. Inst. 37 (2019) 4303–4317. doi:10.1016/j.proci.2018.09.002.

[7] R. Stevens, D. Keairns, R. Newby, M. Woods, Chemical Looping with Oxygen Uncoupling Systems Studies, in: Proc. 2018 NETL CO2 Capture Technol. Proj. Rev. Meet., 2018. https://netl.doe.gov/sites/default/files/netl-file/B-Stevens-NETL-Chemical-Looping-with-Oxygen-Uncoupling.pdf.

[8] A. Nandy, C. Loha, S. Gu, P. Sarkar, M.K. Karmakar, P.K. Chatterjee, Present status and overview of Chemical Looping Combustion technology, Renew. Sustain. Energy Rev. 59 (2016) 597–619. doi:10.1016/j.rser.2016.01.003.

[9] K.M. Merrett, K.J. Whitty, Evaluation of coal conversion pathways in fluidized bed

chemical looping combustion with oxygen uncoupling (CLOU), Fuel. 258 (2019) 116157. doi:10.1016/j.fuel.2019.116157.

[10] P. Wang, N. Means, B.H. Howard, D. Shekhawat, D. Berry, The reactivity of CuO oxygen carrier and coal in Chemical-Looping with Oxygen Uncoupled (CLOU) and In-situ Gasification Chemical-Looping Combustion (iG-CLC), Fuel. 217 (2018) 642–649. doi:10.1016/j.fuel.2017.12.102.

[11] C.K. Clayton, K.J. Whitty, Measurement and modeling of decomposition kinetics for copper oxide-based chemical looping with oxygen uncoupling, Appl. Energy. 116 (2014) 416–423. doi:10.1016/j.apenergy.2013.10.032.

[12] T. Mattisson, Materials for Chemical-Looping with Oxygen Uncoupling, ISRN Chem. Eng. 2013 (2013) 1–19. doi:10.1155/2013/526375.

[13] A. Lyngfelt, B. Leckner, A 1000 MW th boiler for chemical-looping combustion of solid fuels – Discussion of design and costs, Appl. Energy. 157 (2015) 475–487. doi:10.1016/j.apenergy.2015.04.057.

[14] M. Tähtinen, E. Tsupari, J. Kärki, Feasibility and sensitivity of solid fuel CLC plant investment with oxygen carrier recovery, in: 3rd Int. Conf. Chem. Looping, 2014.

[15] US Geological Survey, Mineral Commodity Summeries 2019, 2019. https://www.usgs.gov/centers/nmic/mineral-commodity-summaries.

[16] A. Abad, J. Adánez, F. García-labiano, L.F. De Diego, P. Gayán, J. Celaya, Mapping of the range of operational conditions for Cu- , Fe- , and Ni-based oxygen carriers in chemical-looping combustion, 62 (2007) 533–549. doi:10.1016/j.ces.2006.09.019.

[17] R. Siriwardane, H. Tian, D. Miller, G. Richards, Fluidized bed testing of commercially prepared MgO-promoted hematite and CuO – Fe 2 O 3 mixed metal oxide oxygen carriers

for methane and coal chemical looping combustion, Appl. Energy. 157 (2015) 348–357. doi:10.1016/j.apenergy.2015.04.042.

[18] Z. Reiking, H. Shim, K.J. Whitty, J.S. Lighty, Computational simulation of a 100 kW dual circulating fluidized bed reactor processing coal by chemical looping with oxygen uncoupling, Int. J. Greenh. Gas Control. 90 (2019) 102795. doi:10.1016/j.ijggc.2019.102795.

[19] J. Strohle, P. Ohlemuller, B. Epple, Chemical Looping Pilot Operation in 1 MWth Scale - Lessons Learnt and The Way Forward, in: 5th Int. Conf. Chem. Looping, 2018.

[20] S. Bayham, D. Straub, J. Weber, Operation of a 50-kW th chemical looping combustion test facility under autothermal conditions, Int. J. Greenh. Gas Control. 87 (2019) 211–220. doi:10.1016/j.ijggc.2019.05.022.

[21] H.M. Feilen, Attrition Rate Of Oxygen Carriers In Chemical Looping Combustion Systems, University of North Dakota, 2015.

[22] T. Nelson, J.G. Van Der Watt, D. Laudal, H. Feilen, M. Mann, S. Srinivasachar, Reactive jet and cyclonic attrition analysis of ilmenite in chemical looping combustion systems, Int. J. Greenh. Gas Control. 91 (2019) 102837. doi:10.1016/j.ijggc.2019.102837.

[23] F. Liu, X. Wu, L. Yang, H. Bu, X. Zhang, Evaluation of a bauxite cement-bonded Fe-based oxygen carrier during a hundred of cycles under coal-fueled chemical looping combustion conditions, Fuel Process. Technol. 199 (2020) 106267. doi:10.1016/j.fuproc.2019.106267.

[24] L. Liu, Z. Li, L. Wang, Z. Zhao, Y. Li, N. Cai, MgO-kaolin-supported manganese ores as oxygen carriers for chemical looping combustion looping combustion, Ind. Eng. Chem. Res. (2019). doi:10.1021/acs.iecr.9b05267.

[25] A. Cabello, P. Gayán, L.F. De Diego, A. Abad, J. Adánez, On the attrition evaluation of oxygen carriers in Chemical Looping Combustion, Fuel Process. Technol. 148 (2016) 188–197. doi:10.1016/j.fuproc.2016.03.004.

[26] M. Kamran, J. Hamuyuni, V. Agarwal, J. Pihlasalo, Sulfuric acid leaching for capturing value from copper rich converter slag, J. Clean. Prod. 215 (2019) 1005–1013. doi:10.1016/j.jclepro.2019.01.083.

[27] A. Behnamfard, M. Mehdi, F. Veglio, Process development for recovery of copper and precious metals from waste printed circuit boards with emphasize on palladium and gold leaching and precipitation, Waste Manag. 33 (2013) 2354–2363. doi:10.1016/j.wasman.2013.07.017.

[28] C. Hu, K. Shih, J.O. Leckie, Formation of copper aluminate spinel and cuprous aluminate delafossite to thermally stabilize simulated copper-laden sludge, J. Hazard. Mater. 181 (2010) 399–404. doi:10.1016/j.jhazmat.2010.05.024.

[29] C. Saha, S. Zhang, K. Hein, R. Xiao, S. Bhattacharya, Chemical looping combustion (CLC) of two Victorian brown coals - Part 1: Assessment of interaction between CuO and minerals inherent in coals during single cycle experiment, Fuel. 104 (2013) 262–274. doi:10.1016/j.fuel.2012.08.009.

[30] C. Saha, S. Zhang, R. Xiao, S. Bhattacharya, Chemical looping combustion (CLC) of two Victorian brown coals - Part 2: Assessment of interaction between CuO and minerals inherent in coals during multi cycle experiments, Fuel. 96 (2012) 335–347. doi:10.1016/j.fuel.2012.08.009.

[31] R. Gong, C. Qin, D. He, L. Tan, J. Ran, Oxygen Uncoupling of Cu-Based Oxygen Carrier with the Presence of Coal Ash in Chemical Looping Process, Energy and Fuels. 32 (2018)

7708–7717. doi:10.1021/acs.energyfuels.8b01090.

[32] M. Keller, M. Arjmand, H. Leion, T. Mattisson, Interaction of mineral matter of coal with oxygen carriers in chemical-looping combustion (CLC), Chem. Eng. Res. Des. 92 (2014) 1753–1770. doi:10.1016/j.cherd.2013.12.006.

[33] E. Darwish, D. Yllmaz, H. Leion, Experimental and Thermodynamic Study on the Interaction of Copper Oxygen Carriers and Oxide Compounds Commonly Present in Ashes, Energy and Fuels. 33 (2019) 2502–2515. doi:10.1021/acs.energyfuels.8b04060.

[34] J. Dai, K.J. Whitty, Predicting and alleviating coal ash-induced deactivation of CuO as an oxygen carrier for chemical looping with oxygen uncoupling, Fuel. 241 (2019) 1214–1222. doi:10.1016/J.FUEL.2019.02.029.

[35] J. Dai, K. Whitty, Effects of Coal Ash on CuO as an Oxygen Carrier for Chemical Looping with Oxygen Uncoupling, Energy and Fuels. 32 (2018) 11656–11665. doi:10.1021/acs.energyfuels.8b02521.

[36] R. Pérez-Vega, A. Abad, P. Gayán, F. García-Labiano, M.T. Izquierdo, L.F. De Diego, J. Adánez, Coal combustion via Chemical Looping assisted by Oxygen Uncoupling with a manganese-iron mixed oxide doped with titanium, Fuel Process. Technol. 197 (2020) 106184. doi:10.1016/j.fuproc.2019.106184.

[37] A. Pérez-Astray, I. Adánez-Rubio, T. Mendiara, M.T. Izquierdo, A. Abad, P. Gayán, L.F. de Diego, F. García-Labiano, J. Adánez, Comparative study of fuel-N and tar evolution in chemical looping combustion of biomass under both iG-CLC and CLOU modes, Fuel. 236 (2019) 598–607. doi:10.1016/j.fuel.2018.09.003.

[38] I. Adánez-Rubio, A. Abad, P. Gayán, L.F. de Diego, F. García-Labiano, J. Adánez, Performance of CLOU process in the combustion of different types of coal with CO2

capture, Int. J. Greenh. Gas Control. 12 (2013) 430–440. doi:10.1016/j.ijggc.2012.11.025.

[39] O. Knacke, O. Kubaschewski, K. Hesselmann, Thermochemical properties of inorganic substances, (1991). file://catalog.hathitrust.org/Record/002615188.

[40] M. Mrovec, J. Leitner, M. Nevriva, D. Sedmidubsky, J. Stejskal, Thermochemical properties of MeCuO2 and Me2CuO3 (Me=Ca, Sr, Ba) mixed oxides, Thermochim. Acta. 318 (1998) 63–70.

[41] P.H. Bolt, F.H.P.M. Habraken, J.W. Geus, Formation of Nickel, Cobalt, Copper, and Iron Aluminates from α- and γ-Alumina-Supported Oxides: A Comparative Study, J. Solid State Chem. 69 (1998) 59–69. doi:10.1006/jssc.1997.7590.